Environmental Science Nano

ROYAL SOCIETY OF CHEMISTRY

PAPER

View Article Online
View Journal | View Issue

Cite this: *Environ. Sci.: Nano*, 2022, **9**, 1414

A different protein corona cloaks "true-to-life" nanoplastics with respect to synthetic polystyrene nanobeads†

Serena Ducoli,[ab] Stefania Federici, *[bc] Roland Nicsanu,[d] Andrea Zendrini,[de] Claudio Marchesi,[bc] Lucia Paolini,[de] Annalisa Radeghieri,[de] Paolo Bergese [bde] and Laura E. Depero[bc]

Received 5th November 2021,
Accepted 7th February 2022

DOI: 10.1039/d1en01016f

rsc.li/es-nano

Understanding the impact of nanoplastics on the environment and living organisms is becoming increasingly urgent. Given the complexity of separating nanoplastics from environmental samples, to date fundamental studies are mostly conducted by using model synthetic nanobeads. Here we propose nanoparticles obtained by mechanical fragmentation under cryogenic conditions of daily-life polystyrene plastic items, "true-to-life" nanoplastics (T2LNPs), as a closer model to the real world. T2LNP samples are composed by populations of spheroidal nanoparticles with a broad multimodal size distribution, ranging from a few to hundreds of nanometers, in contrast with their synthetic counterpart, made of monomodal polystyrene spherical nanoparticles (165 nm). In addition, we show that upon incubation with human plasma a different protein corona forms on the T2LNPs with respect to the synthetic nanobeads. Since the protein corona is what the "cell first sees" when interacting with a nanoobject, this suggests that T2LNPs could be a more representative sample for studying the interaction of nanoplastics with biological systems and in turn for evaluating their effect on human health and the environment.

Environmental significance

Nanoplastics are emerging environmental pollutants that are receiving increasing attention. Most of the work done to date to understand nanoplastic interactions with natural and biological systems considers synthetic polystyrene nanobeads as a widespread model of polymers. Nevertheless, despite the fundamental role of these nanomaterials, they share poor analogies with their environmental counterpart. This work aims to understand the nanoscale behaviour of nanoplastic interactions with biological systems through more realistic environmental materials, called "true-to-life" nanoplastics, produced by mimicking the environmental breakdown process. The results show a different protein corona on true-to-life nanoplastics with respect to synthetic nanobeads, highlighting the need to test more environmentally relevant conditions and opening new possibility to understand the impact of nanoplastics on the environment and human health.

Introduction

Environmental plastic pollution is nowadays a great concern. The extremely wide usage of plastic in almost every human activity has led to a progressive accumulation of plastic waste in the environment.[1,2] Once plastic enters the environment, especially oceans and seas, it undergoes abiotic and biotic degradation processes, such as mechanical fragmentation induced by water and marine rock action,[3] photodegradation,[3] and biological metabolism.[4] Plastic degradation results in progressive changes of physical properties (such as crystallinity and mechanical integrity),[5] embrittlement, and fragmentation into smaller pieces, generating micro- and nanoscale particles.[6] The need to understand the possible implications of microplastic and nanoplastic pollution on the environment and living organisms is becoming increasingly urgent.[7]

Even if microplastics have been largely found in nature,[8] often associated with organic and inorganic pollutants,[9–11] demonstrating severe damage to living organisms,[12–14] different considerations must be taken into account for nanoplastics. Studies regarding nanoplastics are growing

[a] *Department of Information Engineering, University of Brescia, Brescia, Italy*
[b] *National Interuniversity Consortium of Materials Science and Technology (INSTM), Florence, Italy*
[c] *Department of Mechanical and Industrial Engineering, University of Brescia, Brescia, Italy. E-mail: stefania.federici@unibs.it*
[d] *Department of Molecular and Translational Medicine, University of Brescia, Brescia, Italy*
[e] *Consorzio Sistemi a Grande Interfase (CSGI), Department of Chemistry, University of Florence, Sesto Fiorentino, Italy*

† Electronic supplementary information (ESI) available. See DOI: 10.1039/d1en01016f

exponentially, but due to the complexity of separating nanoplastics from environmental samples,[15,16] most of the studies conducted so far have been carried out on model nanoparticles, such as synthetic polystyrene nanobeads.[17–21] The toxicity of these synthetic polymeric nanoparticles has been extensively investigated on cells and marine organisms at different trophic levels, evidencing several biological dysfunctions.[22–28] In addition, nanoplastics could be even more dangerous than their micrometric counterpart because, due to nanometric size, they are thought to be able to penetrate tissues and biological barriers.[29,30]

However, despite this bulk of information, several knowledge gaps still exist about the behavior and characteristics of naturally-occurring nanoplastics. Nanobeads synthesized in the framework of colloidal chemistry, following bottom-up approaches, share no analogies with nanoplastics forming in nature, following top-down degradation pathways.[17] Pristine nanoparticles usually are uniform in size, shape, composition, while naturally-occurring nanoplastics are expected to be highly heterogeneous in size, have irregular shapes, and complex surface chemistry (Fig. 1).[31,32] There is an urgent need to create nanomaterials that better reflect the real characteristics of nanoplastics naturally formed, *viz.* true-to-life nanoplastics (T2LNPs), to close the gap between the laboratory parameters and the rules of nature, and to provide more realistic understandings of the characteristics of nanoplastics. To date, some attempts have been made to generate micro- and nanoplastics by fragmentation procedures, following different top-down approaches mimicking the natural processes of environmental degradation.[32–37] These approaches cannot account for all the simultaneous mechanisms that contribute to the degradation of plastic in nature, but represent a step forward in closing the gap in the nanotoxicology of environmental samples.

Nevertheless, interactions of fragmentally generated nanoplastics and biological systems are far from being understood. When a nanoparticle gets in contact with a complex biological environment, its surface is immediately covered by different biomolecules that form a biological corona.[38] Currently, the protein component of this interaction is traditionally the most studied in nanoplastic toxicology.[39–44]

Expanding the environmental dimensions of the protein corona is now growing attention in the bio–nano interaction research field.[45] The eco-corona that forms upon nanomaterials as they enter the environment may include not only proteins, but also a diverse array of other biomolecules and/or natural organic matter, defining a dynamic and complex system. Nevertheless, the prominent role of proteins in receptor engagement and signalling and their established monitoring and structural characterization promote proteins to a key role in studies of eco-coronas. The proteins within the eco-corona are optimal targets to establish the biophysicochemical principles of corona formation and transformation, as well as downstream impacts on nanomaterial uptake, distribution and impacts on the environment. Moreover, the protein corona provides a new identity to nanoparticles and determines their interactions and effects on cells, tissues, and organisms,[38] leading to a unique characteristic compared with natural organic matter.[45]

Research on protein corona formation onto an inorganic nanoparticle surface is extensive, demonstrating that different nanoparticle characteristics, such as chemical identity,[46] size,[47] shape[48] and surface functionalization,[49] can influence the type of protein adsorbed. Against this background, there is no reason for environmental nanoplastics to share the same behavior of synthetic nanobeads.

In this paper, we present a study on T2LNP production and characterization and protein corona formation with respect to synthetic polystyrene nanobeads (hereafter referred

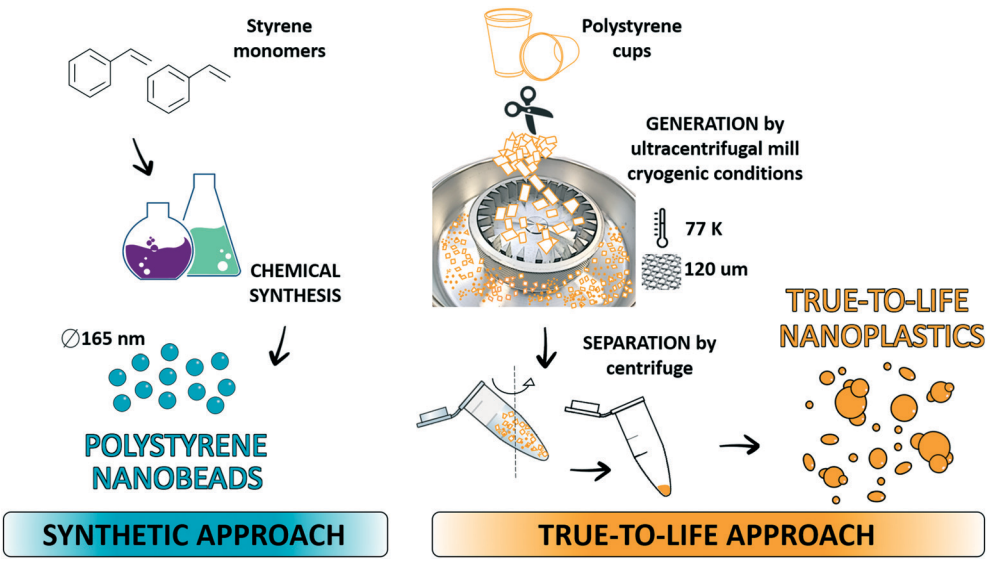

Fig. 1 The synthetic and the true-to-life approaches for generating nanoplastics for controlled experiments.

as nanobeads). First, we investigated the nanoplastic formation from daily life plastic items subjected to mechanical fragmentation through an ultracentrifugal mill operating under cryogenic conditions. Items made of polystyrene were chosen as a close reflection of the composition of the compared nanobeads. The produced nanoplastics were characterized by Fourier transform infrared (FT-IR) spectroscopy to investigate their chemical nature and check the absence of induced chemical modifications. Morphology and size distribution analyses were performed through atomic force microscopy (AFM), giving exciting insights compared to nanobeads. For the biological interaction, human plasma was chosen as a complex biological model fluid for the study of the interactions between inorganic nanoparticles and biomolecules. This fulfills several inherent advantages, including: well characterized and known composition,[50] well established protocols for the corona formation and study,[51] and crucial interest in nanotoxicology.[52] As reported in previous protocols,[46] a temperature of 4 °C was chosen to better preserve the plasma proteins from degradation outside their physiological environment.

Based on these considerations, the protein corona formation from human plasma on T2LNPs and nanobeads was examined, highlighting differences in protein corona compositions.

Materials and methods

Materials

Commonly used polystyrene-based disposable items (coffee cups) were used to produce T2LNP samples by means of mechanical fragmentation. Nanobeads with a nominal diameter of 165 nm were purchased from microParticles GmbH. Nanobeads were diluted at 50 μg ml^{-1} with Milli-Q water immediately before use and characterized by FT-IR spectroscopy and AFM.

Preparation of T2LNP samples

Polystyrene-based disposable items were manually cut with steel scissors, washed with Milli-Q water together with a few drops of commercial detergent and externally sonicated in a water bath for 15 minutes to wash the pieces and remove dirt and grease. Three washing cycles were then performed with Milli-Q water, and then fragments were dried in air at room temperature. Polystyrene pieces were embrittled in liquid nitrogen for 30 minutes, then transferred into an ultracentrifugal mill (ZM 200, Retsch) previously cooled down with liquid nitrogen. Pieces were blended at 18 000 rpm (17 963*g*) until complete fragmentation (about 60 seconds) under a continuous flow of liquid nitrogen to avoid overheating of the rotor with consequent degradation of the polymer. The mill was equipped with a 120 μm mesh sieve, acting as a first fractionation step for nanoplastics. The powder was collected and stored in a falcon tube.

Pre-treatment of Milli-Q water

All experiments were conducted in centrifuged Milli-Q water. The preparation of Milli-Q water is a crucial step to avoid unknown contamination in the final concentrated pellet of T2LNPs. Milli-Q water was carefully pre-treated before use by centrifugation at 16 000*g* for 45 minutes (Avanti J25, rotor JA20, polycarbonate tubes 357003 Beckman) to separate all the interfering suspended particles. The supernatant was collected leaving 1 cm of Milli-Q water so as not to disturb the pelleted material.

Separation and concentration of T2LNPs

About 0.4 g of powder originating from the fragmentation procedure was suspended in pre-treated Milli-Q water and externally sonicated in a water bath for about 30 minutes. To recover and concentrate T2LNPs from the medium, a series of centrifugation steps were applied. Samples were subjected to two sequential centrifugation steps. The first step was conducted at 500*g* for 45 minutes (5804R Eppendorf centrifuge, A-4-44 rotor, 50 mL 174 × 22 mm polypropylene tube Sarstedt). Supernatants were transferred into new centrifuge tubes and then centrifuged at 16 000*g* for 45 minutes (Avanti J25, rotor JA20, polycarbonate tubes 357003 Beckman); pellets were preserved while supernatants were discarded.

T2LNP characterization by FT-IR spectroscopy

FT-IR measurements were performed with an Equinox 55 spectrometer (Bruker) operating in transmission mode. Pellets of T2LNPs were resuspended in Milli-Q water and briefly sonicated in a water bath for 5 minutes to promote nanoparticle resuspension. From each sample a 2 μL droplet was deposited onto a diamond window and dried under a mild stream of nitrogen. Measurements were performed at a nominal resolution of 4 cm^{-1} in the range of 4000–400 cm^{-1}. To increase the signal-to-noise ratio, 128 scans per sample were co-added without changing the position of the sample between each scan (time per scan 0.9 seconds, included dead time). For all spectra manipulations OPUS software 5.0 was used.

T2LNP morphological characterization with AFM

Pellets of T2LNPs were resuspended in Milli-Q water and briefly sonicated in a water bath for 5 minutes to promote nanoparticle resuspension. Three μl of the samples were spotted on a freshly cleaved round-shaped mica sheet (grade V-1, thickness 0.1 mm, diameter 10 mm) and air-dried over a heating plate at 37–40 °C (Velp Scientifica). Dried samples were then imaged in tapping mode with a JSPM-4210 AFM microscope (JEOL) equipped with NSC35/ALBS (MikroMasch) ultrasharp tips (resonant frequency ≈ 205 kHz; force constant ≈ 8.9 N m^{-1}, typical radius tip <10 nm). Topography images were collected over different length scales (scan size ranged from 2 μm to 25 μm with a scan speed

ranging from 9.23 μm s^{-1} to 46.2 μm s^{-1}). The obtained topography images were processed with WSxM 5.0 software[53] and Gwyddion software. The same AFM protocol was also applied for the AFM images of T2LNPs after the formation of the protein corona.

Size distribution analysis of T2LNP samples

Size distribution analysis was performed using AFM images. Briefly, images of different length scale (from 2 μm to 25 μm) were obtained by AFM as previously described; images of different length scale were necessary to cover the extremely high polydispersity of the T2LNP samples and considered both single particles and big aggregates. Images were processed using Gwyddion software. About 20 000 items were counted for size distribution and both the *z*-dimension (height) and the diameter of particles were selected for the analysis to avoid tip-driven AFM artefacts and to account also for in-plane T2LNP aggregates. Two different independent T2LNP samples were analyzed, and data were collected for the final distribution.

Human blood collection and plasma preparation

Protocols were adapted from ref. 51. For details, please refer to the ESI.†

Protein corona formation

Pellets of T2LNPs were resuspended in Milli-Q water, briefly sonicated in a water bath for 5 minutes to promote nanoparticle resuspension, and incubated with plasma diluted 1 : 2 in Milli-Q water for 1 h at 4 °C.

The temperature was chosen to better preserve the plasma proteins from degradation, hydrolysis, outside the physiological conditions. After incubation, samples were diluted 1 : 2 with Milli-Q water and centrifuged at 16 000*g* for 45 minutes at 4 °C (5417C Eppendorf centrifuge, 45-30-11 rotor) to pellet the nanoparticle–protein complexes and separate from the supernatant plasma. Pellets were then subjected to three washing steps by resuspending in 500 μl of Milli-Q water and centrifuging at 16 000*g* for 45 minutes at 4 °C. Pellets were then stored at 4 °C for AFM, FT-IR, and SDS-PAGE experiments.[54]

The same protocol was also applied to nanobead samples with a concentration of 10 μg ml^{-1}, 25 μg ml^{-1} and 50 μg ml^{-1}.

SDS-PAGE of protein corona samples

After the third washing step, pellets were resuspended in 20 μl of Milli-Q water and briefly sonicated in a water bath for 5 minutes. Four μl of reducing sample buffer 6× (480 mM tris-HCl pH 6.8; 12% SDS; 45% glycerin; 0.06% bromophenol blue, 12%-mercaptoethanol) were added, and the samples were boiled at 95 °C for 5 minutes. Samples were loaded in 7.5% polyacrylamide gel (30% acrylamide and bis-acrylamide solution, 29 : 1 Bio-Rad). Gel electrophoresis was performed at 140 V, for about 60 min. Gels were stained with Imperial protein stain (Thermo-Fisher Scientific) for 2 h at room temperature and then destained in Milli-Q water overnight at room temperature. The absence of non-specific signals arising from bare T2LNPs and nanobeads was also checked by SDS-PAGE analysis. Images were acquired using a G:Box Chemi XT Imaging system.[55] For densitometric analysis, the Gene Tools (Syngene, UK) software was used to compare the protein corona adsorbed on the T2LNP and nanobead surface.

Results and discussion

T2LNP production by mechanical fragmentation

Mechanical fragmentation was chosen among several methods to produce T2LNPs, mimicking the natural plastic degradation processes caused by rocks and water erosion forces. This fragmentation process was carried out using an ultracentrifugal mill, which allows rapid polymer fragmentation, with the great advantage of preserving the sample from environmental contaminants and allowing the process to be regulated. However, the well-known disadvantage of this method is the generation of local heat, causing thermal degradation of the polymer. For this reason, the samples have been kept under cryogenic conditions during the fragmentation. Before the milling procedure, the plastic items have been embrittled in liquid nitrogen for 30 minutes.

Before the separation and centrifugation steps, the fragmented pieces were suspended in Milli-Q water. The proper pre-treatment of Milli-Q water represented a crucial step to avoid contamination. Fig. S1a–c in the ESI† show the AFM images of untreated control water following the same concentration steps as T2LNPs where contaminant nanoparticles are detected. The mandatory need to obtain pure preparations of T2LNPs led to water pre-treatment to remove any contaminants, as shown in Fig. S1d–f in the ESI.†

T2LNP characterization by FT-IR spectroscopy

Vibrational spectroscopic techniques are recognized as valuable methods for plastic identification. For example, in plastic recycling plants, vibrational spectroscopy techniques are the basis of automated processes for plastic type sorting, in place of or in combination with manual separation, which is time-consuming and more prone to errors.[56] Mid-infrared transmission spectroscopy is widely used for bulk polymers for both qualitative and quantitative analysis,[57] and it is also considered an accurate technique to investigate biological materials.[58] It provides unique fingerprint spectra, using wavelengths ranging from 4000 cm^{-1} to 400 cm^{-1}. Near-infrared spectroscopy (NIR), using wavelengths ranging from 780 nm to 2500 nm, is gaining attention thanks to the development of miniaturized, portable, and real-time NIR spectrometers.[59] Raman spectroscopy is also used for its greater simplicity in preparing the sample to be analyzed. While wide overtone bands can be obtained with NIR spectroscopy, Raman spectroscopy has the advantage of sharper and more well-resolved bands.[60] However, it has

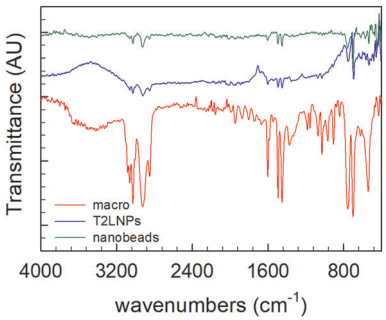

Fig. 2 FT-IR spectra, collected in transmission mode, of polystyrene macro pieces (red spectrum), T2LNPs (blue spectrum) and nanobeads (green spectrum).

some limits, especially with non-homogeneous powdered samples and colloidal suspensions.[57]

T2LNP samples were analyzed by FT-IR spectroscopy operating in transmission mode. Fig. 2 shows FT-IR spectra recorded on parental polystyrene macro pieces, fragmented T2LNPs and nanobeads. The spectrum of macro pieces displays characteristic polystyrene absorption bands, namely, peaks at 3083, 3060 and 3027 cm^{-1}, corresponding to aromatic C–H stretching vibrations; peaks at 2925 cm^{-1} and 2852 cm^{-1}, corresponding to the asymmetric and symmetric stretching vibrations of methyl ($–CH_3$) and methylene ($–CH_2$) groups; a peak at 1602 cm^{-1}, corresponding to aromatic ring stretching vibrations; and peaks at 1492 cm^{-1} and 1452 cm^{-1}, corresponding to the asymmetric and symmetric bending vibrations of methyl ($–CH_3$) and methylene ($–CH_2$) groups and to aromatic ring stretching vibrations.[61,62] FT-IR analysis revealed the presence of the typical peaks also in fragmented T2LNP samples, confirming the chemical fingerprint. Due to the low concentration of T2LNP samples, some absorption peaks are lost, and the intensity of the main absorption bands is lower compared to that of the bulk material, but it is possible to clearly observe C–H characteristic stretches at 3085, 3060 and 3029 cm^{-1}, methyl and methylene stretches at 2920 and 2852 cm^{-1}, an aromatic ring stretch at 1602 cm^{-1} and methyl and methylene bending, together with aromatic ring stretches at 1492 and 1452 cm^{-1}. This behavior was also confirmed for nanobead samples. FT-IR analysis confirmed the presence of chemically intact polymer after the fragmentation procedure without induced degradation. Mechanical fragmentation coupled with the use of liquid nitrogen is essential to preserve the chemical nature of the T2LNPs and avoiding degradations (see Fig. S2 in the ESI† for an example of polymer degradation after using a not suitable protocol of mechanical fragmentation with a time of embrittlement restricted to 10 minutes and without a continuous flow of liquid nitrogen during the process).

Morphological characterization and size distribution of T2LNPs

AFM was used to investigate the morphology of single particles and aggregates in the T2LNP samples. AFM was also employed to determine the size distribution, taking advantage of non-monodispersed solutions over traditional optical correlation techniques, such as dynamic light scattering (DLS) and nanoparticle tracking analysis (NTA).[63] It has been demonstrated that the sample polydispersity can distort DLS results since the population of big particles in the sample can screen the smaller ones.[64] On the other hand, NTA tracks the movement of single particles, so it better determines the size even in polydisperse systems. However, many studies report that few large particles negatively affect the detection of smaller ones, reducing their quantification up to 80%.[65,66] Furthermore, studies on the accuracy of these analytical tools are usually conducted by mixing a few populations of well-defined different sized nanoparticles. In contrast, in the case of the T2LNP sample, we expect a large variability in size, from particles of a few nanometers to large aggregates of hundreds of nanometers; therefore, the accuracy and reliability of such measurements could be further compromised. Lastly, the NTA requires the presence of specialized operators and is strongly influenced by the manual skills of the operator, as well as by the type of instrument, software and calibration used.[67]

Topography AFM images were acquired at different length scales to extrapolate the size distribution and the shapes of the T2LNPs. Fig. 3 shows the representative images recorded with a scan size set to 25 μm (a–c), 10 μm (d–f), 5 μm (g–i), and 2 μm (j–l). The most populated fraction of the T2LNP sample has a size of a few tens of nanometers. The mismatch in the *z*-dimension and diameter observed for some round-shaped particles suggests the aggregation of nanoparticles with a resultant tip-sample convolution effect, and/or the presence of elongated particles.[36] Aggregates of different sizes and shapes are also clearly detected, reaching in some cases a dimension larger than 1 μm in diameter.

Two different T2LNP samples independently prepared were analyzed, summing up to 20 000 particles giving a strong and statistically representative distribution. Both diameter and *z*-dimension parameters were measured, considering the presence of in-plane aggregates or elongated particles, as suggested from topography images, to avoid tip-driven AFM artifacts.

Fig. 4 shows the overall AFM size distribution data of the two analyzed preparations of T2LNPs highlighting the predominance of small particles, below 100 nm in *x*-, *y*- and *z*-dimensions, according to the topography data. The size distribution shows the median values of the *z*-dimension and diameters of 7.5 nm and 24.0 nm, respectively. The mean values for the *z*-dimension and diameter, more affected by the presence of big aggregates, are (13.5 ± 0.2) nm and (43.0 ± 0.5) nm, respectively.

The study of nanoplastics derived from environmental samples is still in its infancy, due to several technical drawbacks related to their isolation and purification. Recently, some remarkable attempts have been made to isolate nanoplastics from environmental samples,[68] but dimensional analysis in most cases has been affected by

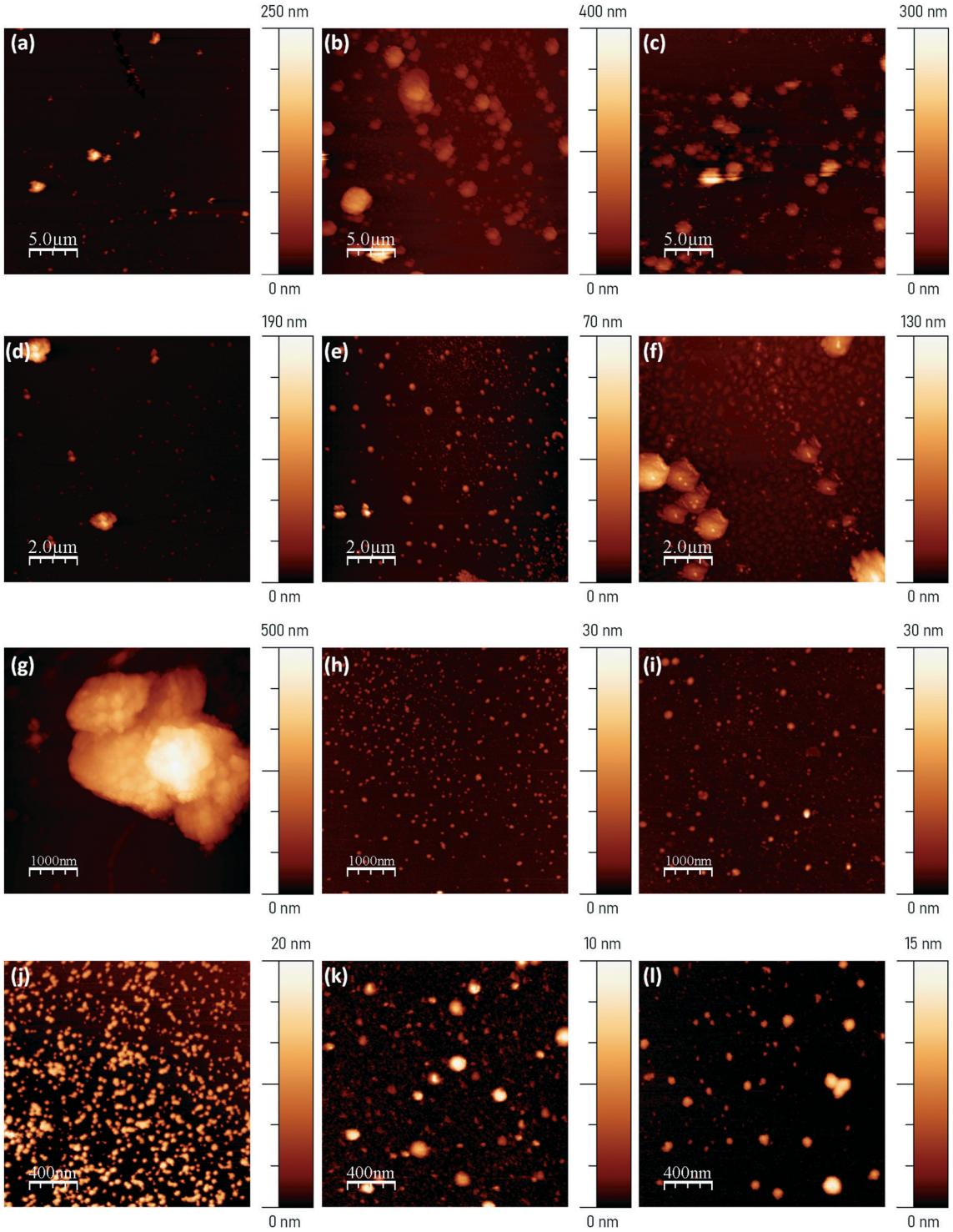

Fig. 3 Atomic force microscopy (AFM) topography images of T2LNPs adsorbed on mica, with a scan size of 25 μm (a–c), 10 μm (d–f), 5 μm (g–i), and 2 μm (j–l), and scale bars as indicated. Colorimetric scales indicate the maximum height for each image.

excessive dilution of nanoplastics[69] or by the interference of natural contaminants.[70] An interesting study has recently isolated nanoplastics of PE, PS and PVC from soil and provided a size-distribution analysis using asymmetric flow-field flow fractionation coupled with UV spectroscopy and static light scattering (AF4-UV-SLS): the major part of the recovered nanoplastics was in the range of 20–150 nm,[71] in fair agreement with the size distribution we have obtained in this work.

To further highlight the significance of the presented study, an inter-sample analysis was also performed, by comparing the two different T2LNP samples. Size

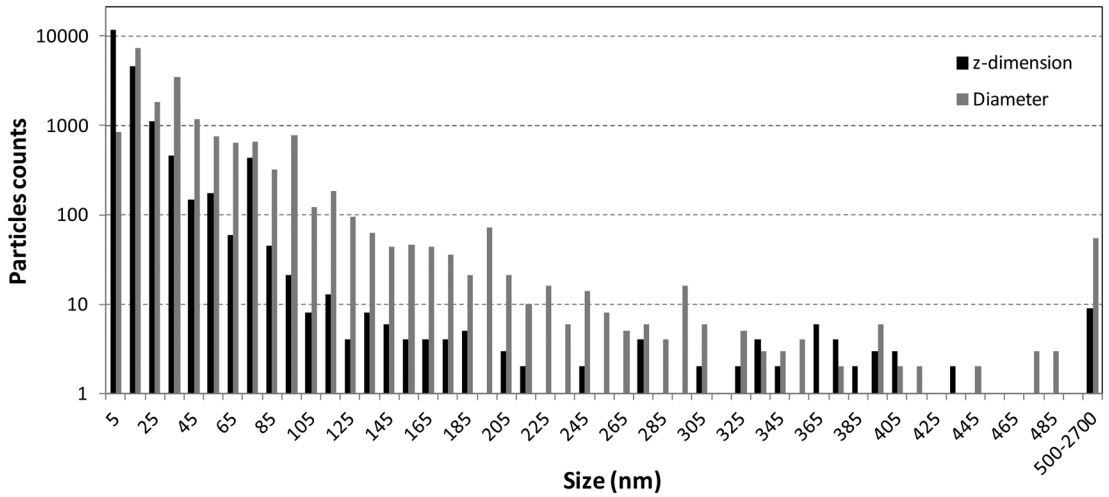

Fig. 4 Size distribution obtained from AFM images of two independent preparations of T2LNPs. A grand total of 18 678 objects were analyzed (*y* axis, log scale).

distributions and statistical details (Fig. S4 and Table S1 in the ESI†) provide the median values of the *z*-dimension of 6.8 nm for the first sample and 8.0 nm for the second one. In comparison, the median values of the diameter are 22.9 nm and 27.6 nm for the two samples. The mean values of the *z*-dimension and diameter are (14.2 ± 0.2) nm and (41.3 ± 0.5) nm, respectively, for the first sample, and (12.9 ± 0.3) nm and (44.7 ± 0.8) nm, respectively, for the second sample. These data confirm the repeatability of the T2LNP production process by mechanical fragmentation, with a strong predominance of particles with a diameter smaller than 100 nm.

In Fig. S3 in the ESI† a representative AFM topography image of nanobeads is reported, clearly showing a regular particle distribution and a uniform size of about 165 nm (*z*-scale).

Protein corona on T2LNPs and nanobeads

After determining the morphological diversity between T2LNPs and nanobeads, we investigated their ability to interact with biological environments. Given the fundamental role of the protein corona in defining the final identity of the nanoparticles and their communication interface,[38] we compared the protein corona adsorbed on the T2LNP and nanobead surface after their incubation with human plasma. To investigate this interaction, T2LNPs and nanobeads were incubated with plasma diluted 1 : 2 in Milli-Q water for 1 h at 4 °C. After incubation, samples were diluted 1 : 2 with Milli-Q water, centrifuged and washed as described in the Materials and methods section.

The first analysis of the protein corona molecules was performed by FT-IR measurements. The spectra are shown in Fig. S5 in the ESI† and confirmed the presence of the protein film, showing the characteristic absorption bands ascribed to amide I and amide II bands around 1650 cm^{-1} and 1540 cm^{-1}, primarily due to the carbonyl stretching vibration and N–H bending vibrations,[72] respectively. A further morphological check was performed by AFM. The topography images did not show significant modifications of the morphologies, neglecting the contribution of the protein thin film on the T2LNP surface (Fig. S6 ESI†). This result was expected since the protein corona in the literature is described as a thin layer with a thickness of a few nanometers, corresponding in some cases to a protein monolayer.[40,73] For this reason, differences in the nanoparticle diameter before and after the formation of the protein corona is unlikely to be detected.

To visualize the differences in the protein composition of the corona adsorbed on T2LNPs and nanobeads, the samples were heated in reducing sample buffer, separated by SDS-PAGE electrophoresis on acrylamide/bisacrylamide gel and stained with Imperial stain (Fig. 5a). A plasma sample, not previously incubated with nanoparticles, was processed in parallel and used as a negative control (CTRL−) to check the non-specific signal due to the protein interaction with plastic tubes. Possible background signals arising from T2LNPs and nanobeads were also checked by SDS-PAGE analysis; the result in Fig. 5b rules out any interference from nanoplastics. SDS-PAGE allowed separation of proteins based on their molecular weight and the resulting protein bands in the gel were stained using a Coomassie brilliant blue-based dye. At first glance, the profile of the protein corona adsorbed on T2LNPs is strikingly different in comparison with the profile of nanobeads, and both do not mirror the plasmatic total protein pattern (plasma).

In addition, CTRL− showed lower signal intensity and a profile less rich in bands compared to all the other samples, highlighting the specificity of the signals in T2LNP and nanobead lanes.

Moreover, some protein bands that are low concentrated in plasma are selectively enriched in the two protein coronas (blue stars). On the other hand, other protein bands abundant in plasma have a less intense signal in the two

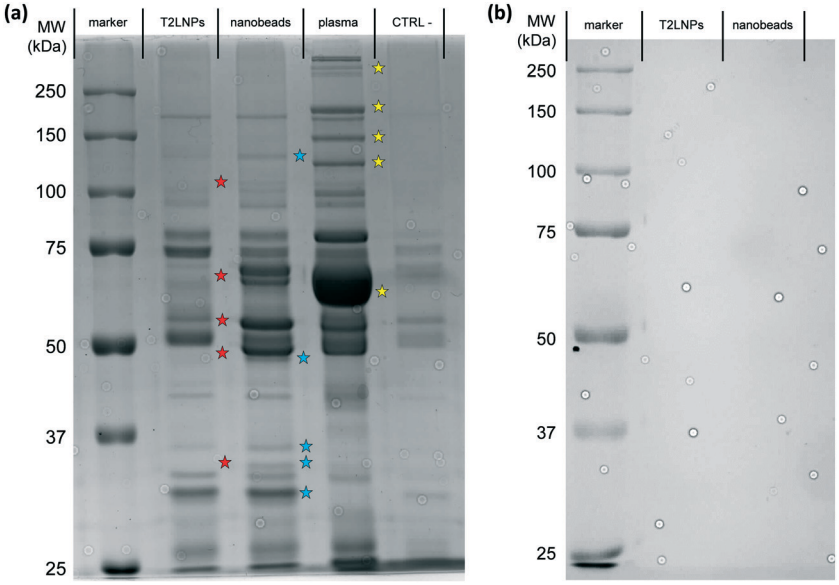

Fig. 5 a) SDS-PAGE analysis of the protein corona adsorbed on T2LNPs and nanobeads after human plasma incubation, human plasma (plasma, 20 μg) and human plasma subjected to the same incubation/centrifugation protocol as T2LNPs and nanobeads, but without nanoparticles (CTRL–). All samples were subjected to SDS-PAGE using 7.5% acrylamide gel and stained with Imperial stain. Differences in protein patterns are highlighted with stars as described in the text. The image is representative of three independent experiments. b) Control SDS-PAGE performed on bare T2LNPs and nanobeads rules out any interference from nanoplastics.

nanomaterial samples (yellow stars). Albumin is the most representative case. It is the most abundant protein in blood plasma, representing approximately 55% of total blood proteins. It has a molecular weight of 66.5 kDa and clearly emerges from the SDS-PAGE analysis on plasma. However, in the protein patterns of the two nanomaterial–protein complexes, only a less intense signal can be observed (almost absent in the case of the T2LNPs). These findings are in full agreement with the literature. In fact, although some studies of the interaction between albumin and nanobeads show the formation of a protein corona,[39,74] a different behavior is experienced in testing a complex fluid, such as human plasma. In this case, it was shown that the predominant proteins in the corona are mainly the three subunits α-, β- and γ- of fibrinogen, while albumin represents a small percentage of the total amount of bound proteins.[46,75]

The differences in protein corona profiles of T2LNPs and nanobeads are highlighted in Fig. 5 with red stars and can be

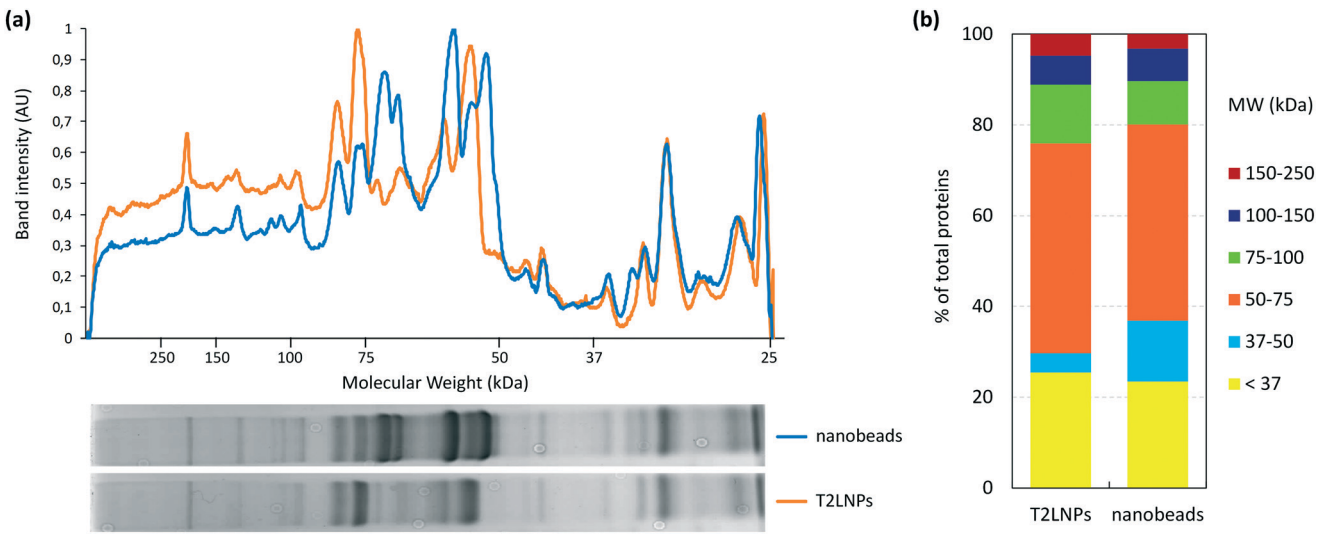

Fig. 6 a) Densitometric profiles of the protein corona adsorbed on T2LNPs (orange line) and on nanobeads (blue line). b) Densitometric profile data elaboration shows the relative abundance (% of total proteins) of the different molecular weight groups (M_W), with respect to the total amount of proteins for each lane (T2LNPs and nanobeads).

even better observed by analyzing the densitometric profile of the two lanes, respectively (Fig. 6a). The greatest differences in the densitometric profiles can be observed in the range between 150 and 50 kDa where some proteins are selectively adsorbed either on T2LNPs or on nanobeads (Fig. 6a). In addition, densitometric profile data elaboration, showing the relative abundances of proteins grouped on the basis of their molecular weight (Fig. 6b), highlighted that both coronas are formed mostly by proteins with a mass <75 kDa, even if the relative abundance of the different molecular weight groups, with respect to the total amount of protein, is different (46.2% (M_W 50–75 kDa), 4.2% (M_W 37–50 kDa), and 25.4% (M_W < 37 kDa) and 43.2% (M_W 50–75 kDa), 13.3% (M_W 37–50 kDa), and 23.5% (M_W < 37 kDa) for T2LNPs and nanobeads, respectively) (Fig. 6b).

Quantifying T2LNP samples is a state-of-the-art analytical challenge of the field. For this reason, T2LNP and nanobead protein corona signals on SDS-PAGE in Fig. 5a are not normalized to T2LNP and nanobead concentrations. The binding of proteins to nanoparticles is affected by the surface it encounters, and to better assess the effect of the nanoparticle dose on corona formation, three different concentrations of nanobeads (10 μg ml^{-1}, 25 μg ml^{-1} and 50 μg ml^{-1}) were incubated in human plasma and analyzed for protein corona formation. The result of this analysis is reported in Fig. S7 in the ESI† and clearly demonstrates that changes in the nanobead concentration do not affect the type of protein that interact with the nanobead surface, but only the intensity of signals (*i.e.*, the number of proteins), which increases as the nanobead concentration increases.

In summary, these results demonstrate the need of a more representative sample to study the nanoplastic–bio interactions of environmental NPs.

Conclusions

The number of studies reporting the effects of nanoplastics on biota is growing exponentially, and they are commonly based on the use of synthetic nanobeads as models for nanoplastics. These particles have been of utmost importance to standardize methodologies and begin to unravel the fundamental mechanisms of interaction of nanoplastics with biological systems. Nevertheless, there is a strong need to integrate field and laboratory data and test more environmentally relevant conditions,[15] and to define a standard reference sample that mirrors the chemical composition and the variety in morphology and size of naturally-occurring nanoplastics, yet maintaining reasonably narrow production repeatability and physicochemical characteristics.[76]

In this work, we propose a "true-to-life" nanoplastic (T2LNP) reference sample produced by replicating the breakdown process originating in nature due to mechanical forces by mechanical fragmentation under cryogenic conditions of polystyrene-based daily-life items.

The features recorded in AFM topography images showed spheroidal nanoparticles, with a strong predominance of tiny particles of a few tens of nanometers, also combined with aggregates and bigger particles. The richness of information obtained also confirmed AFM as a valuable technique to characterize the size distribution of nanoplastics. The bio–nano interface was investigated through the formation of the protein corona from human plasma both on the T2LNP and nanobead surface, highlighting the different protein profiles for the two nanomaterials. The composition and structure of the protein corona are strictly connected to the chemistry and nanoparticle surface features. There are strong indications that the curvature radius of the nanoparticle is also a key parameter. Fine details of size, shape and bare-surface physicochemical properties can lead to different protein coronas[77] and further characterization at different levels needs to be performed to define the major contributors to the differences between the protein corona formed on T2LNPs and nanobeads.[78] Nevertheless, the differences detected in the two protein corona profiles confirm the gap between controlled models and the complexity in real-life scenarios, supporting the need to develop true-to-life materials as reasonable models for environmental nanoplastics. Given that the protein corona mediates the interaction with biological systems and the surroundings, different compositions of protein corona strongly influence the potential risks of NP pollution for the environment and human health.

The composition of protein corona adsorbed on nanobeads is well documented in the literature, not only with regard to bare nanobeads, but also to functionalized nanobeads (carboxylated polystyrene nanobeads and amine-modified polystyrene nanobeads).[49,75,79] In the present proof-of-concept study, differences in the protein corona between T2LNPs and nanobeads have been demonstrated; a more sensitive proteomic analysis, such as mass spectrometry, will provide a specific analysis of the composition and related physiological functions of the adsorbed protein . This could provide better insight on these differences and their biological implications, helping in understanding the effects of nanoplastics on biota.

Moreover, human plasma was chosen as a well characterized biological model fluid, with established protocols and toxicological relevance; from an environmental point of view that aims at testing the T2LNP behavior under more environmentally relevant conditions, the formation of an eco-corona (from the interaction of T2LNPS with natural organic matter – NOM) could be of utmost importance, also in view of *in vitro* and *in vivo* toxicological tests. Beyond biological/toxicological studies, a more focused physicochemical characterization of T2LNPs is necessary to better determine the reference material characteristics and to allow the repeatability and comparison among future studies. Furthermore, polystyrene nanobead investigations represent almost all available studies; a wider vision that considers also T2LNPs derived from other plastic types could provide more accurate and comprehensive insight into plastic pollution effects.

In conclusion, the broad heterogeneity in size and shape shown by fragmented T2LNPs gives the nanomaterial a peculiar and different behavior compared to the defined pristine nature of nanobeads, nominating T2LNPs as a more representative material for naturally-occurring nanoplastics and opening the possibility to new and unexpected results in biological interactions.

Author contributions

Conceptualization, S. F.; formal analysis, C. M.; funding acquisition, L. E. D., P. B.; investigation, S. D., R. N., L. P., A. Z.; methodology, S. D., L. P., A. R.; resources, L. E. D., P. B.; supervision, S. F., P. B.; visualization: S. D., L. P, A. R., A. Z.; writing – original draft, S. D., S. F., P. B.; writing – review and editing, S. F., P. B., L. P., A. R.

Conflicts of interest

There are no conflicts to declare.

Acknowledgements

This article is based upon work from COST Action CA20101 Plastics monitoRIng detectiOn RemedIaTion recoverY – PRIORITY, supported by COST (European Cooperation in Science and Technology). www.cost.eu. The research was funded by PON "R&I" 2014–2020: SIRIMAP—SIstemi di Rilevamento dell'Inquinamento MArino da Plastiche e successivo recupero-riciclo (No. ARS01_01183, CUP D86C18000520008) and by the National Interuniversity Consortium of Materials Science and Technology (INSTM) through internal funds.

References

1 UNEP, *Marine plastic debris and microplastics – Global lessons and research to inspire action and guide policy change*, 2016.
2 R. Geyer, J. R. Jambeck and K. L. Law, Production, use, and fate of all plastics ever made, *Sci. Adv.*, 2017, **3**, 25–29.
3 A. L. Andrady, Microplastics in the marine environment, *Mar. Pollut. Bull.*, 2011, **62**, 1596–1605.
4 A. L. Dawson, S. Kawaguchi, C. K. King, K. A. Townsend, R. King, W. M. Huston and S. M. Bengtson Nash, Turning microplastics into nanoplastics through digestive fragmentation by Antarctic krill, *Nat. Commun.*, 2018, **9**, 1–8.
5 A. L. Andrady, The plastic in microplastics: A review, *Mar. Pollut. Bull.*, 2017, **119**, 12–22.
6 L. Wang, W. M. Wu, N. S. Bolan, D. C. W. Tsang, Y. Li, M. Qin and D. Hou, Environmental fate, toxicity and risk management strategies of nanoplastics in the environment: Current status and future perspectives, *J. Hazard. Mater.*, 2021, **401**, 123415.
7 D. M. Mitrano, P. Wick and B. Nowack, Placing nanoplastics in the context of global plastic pollution, *Nat. Nanotechnol.*, 2020, **16**, 115–147.
8 L. Peng, D. Fu, H. Qi, C. Q. Lan, H. Yu and C. Ge, Micro- and nano-plastics in marine environment: Source, distribution and threats — A review, *Sci. Total Environ.*, 2020, **698**, 134254.
9 F. G. Torres, D. C. Dioses-Salinas, C. I. Pizarro-Ortega and G. E. De-la-Torre, Sorption of chemical contaminants on degradable and non-degradable microplastics: Recent progress and research trends, *Sci. Total Environ.*, 2021, **757**, 143875.
10 A. Banerjee and W. L. Shelver, Micro- and nanoplastic induced cellular toxicity in mammals: A review, *Sci. Total Environ.*, 2021, **755**, 142518.
11 Y. L. Liao and J. Y. Yang, Microplastic serves as a potential vector for Cr in an in-vitro human digestive model, *Sci. Total Environ.*, 2020, **703**, 134805.
12 M. Cole, P. Lindeque, C. Halsband and T. S. Galloway, Microplastics as contaminants in the marine environment: A review, *Mar. Pollut. Bull.*, 2011, **62**, 2588–2597.
13 L. G. A. Barboza, A. Dick Vethaak, B. R. B. O. Lavorante, A. K. Lundebye and L. Guilhermino, Marine microplastic debris: An emerging issue for food security, food safety and human health, *Mar. Pollut. Bull.*, 2018, **133**, 336–348.
14 J. N. Hahladakis, C. A. Velis, R. Weber, E. Iacovidou and P. Purnell, An overview of chemical additives present in plastics: Migration, release, fate and environmental impact during their use, disposal and recycling, *J. Hazard. Mater.*, 2018, **344**, 179–199.
15 M. Oliveira and M. Almeida, The why and how of micro(nano)plastic research, *TrAC, Trends Anal. Chem.*, 2019, **114**, 196–201.
16 B. Nguyen, D. Claveau-Mallet, L. M. Hernandez, E. G. Xu, J. M. Farner and N. Tufenkji, Separation and Analysis of Microplastics and Nanoplastics in Complex Environmental Samples, *Acc. Chem. Res.*, 2019, **52**, 858–866.
17 J. Gigault, A. ter Halle, M. Baudrimont, P. Y. Pascal, F. Gauffre, T. L. Phi, H. El Hadri, B. Grassl and S. Reynaud, Current opinion: What is a nanoplastic?, *Environ. Pollut.*, 2018, **235**, 1030–1034.
18 J. Wu, R. Jiang, W. Lin and G. Ouyang, Effect of salinity and humic acid on the aggregation and toxicity of polystyrene nanoplastics with different functional groups and charges, *Environ. Pollut.*, 2019, **245**, 836–843.
19 L. Liu, K. Xu, B. Zhang, Y. Ye, Q. Zhang and W. Jiang, Cellular internalization and release of polystyrene microplastics and nanoplastics, *Sci. Total Environ.*, 2021, **779**, 146523.
20 K. Tallec, O. Blard, C. González-Fernández, G. Brotons, M. Berchel, P. Soudant, A. Huvet and I. Paul-Pont, Surface functionalization determines behavior of nanoplastic solutions in model aquatic environments, *Chemosphere*, 2019, **225**, 639–646.
21 O. Oriekhova and S. Stoll, Heteroaggregation of nanoplastic particles in the presence of inorganic colloids and natural organic matter, *Environ. Sci.: Nano*, 2018, **5**, 792–799.
22 X. Sun, B. Chen, Q. Li, N. Liu, B. Xia, L. Zhu and K. Qu, Toxicities of polystyrene nano- and microplastics toward

marine bacterium Halomonas alkaliphila, *Sci. Total Environ.*, 2018, **642**, 1378–1385.

23 W. Lin, R. Jiang, S. Hu, X. Xiao, J. Wu, S. Wei, Y. Xiong and G. Ouyang, Investigating the toxicities of different functionalized polystyrene nanoplastics on Daphnia magna, *Ecotoxicol. Environ. Saf.*, 2019, **180**, 509–516.

24 W. Zhang, Z. Liu, S. Tang, D. Li, Q. Jiang and T. Zhang, Transcriptional response provides insights into the effect of chronic polystyrene nanoplastic exposure on Daphnia pulex, *Chemosphere*, 2020, **238**, 124563.

25 A. T. B. Guimarães, F. N. Estrela, A. S. de L. Rodrigues, T. Q. Chagas, P. S. Pereira, F. G. Silva and G. Malafaia, Nanopolystyrene particles at environmentally relevant concentrations causes behavioral and biochemical changes in juvenile grass carp (Ctenopharyngodon idella), *J. Hazard. Mater.*, 2021, **403**, 123864.

26 T. Ö. Sökmen, E. Sulukan, M. Türkoğlu, A. Baran, M. Özkaraca and S. B. Ceyhun, Polystyrene nanoplastics (20 nm) are able to bioaccumulate and cause oxidative DNA damages in the brain tissue of zebrafish embryo (Danio rerio), *Neurotoxicology*, 2020, **77**, 51–59.

27 C. W. Yu, T. C. Luk and V. H. C. Liao, Long-term nanoplastics exposure results in multi and trans-generational reproduction decline associated with germline toxicity and epigenetic regulation in Caenorhabditis elegans, *J. Hazard. Mater.*, 2021, **412**, 125173.

28 Y. Yang, Q. Wu and D. Wang, Dysregulation of G protein-coupled receptors in the intestine by nanoplastic exposure in Caenorhabditis elegans, *Environ. Sci.: Nano*, 2021, **8**, 1019–1028.

29 K. Yin, Y. Wang, H. Zhao, D. Wang, M. Guo, M. Mu, Y. Liu, X. Nie, B. Li, J. Li and M. Xing, A comparative review of microplastics and nanoplastics: Toxicity hazards on digestive, reproductive and nervous system, *Sci. Total Environ.*, 2021, **774**, 145758.

30 C. C. Gaylarde, J. A. Baptista Neto and E. M. da Fonseca, Nanoplastics in aquatic systems - are they more hazardous than microplastics?, *Environ. Pollut.*, 2021, **272**, 115950.

31 J. Gigault, H. El Hadri, B. Nguyen, B. Grassl, L. Rowenczyk, N. Tufenkji, S. Feng and M. Wiesner, Nanoplastics are neither microplastics nor engineered nanoparticles, *Nat. Nanotechnol.*, 2021, **16**, 501–507.

32 D. Magrì, P. Sánchez-Moreno, G. Caputo, F. Gatto, M. Veronesi, G. Bardi, T. Catelani, D. Guarnieri, A. Athanassiou, P. P. Pompa and D. Fragouli, Laser ablation as a versatile tool to mimic polyethylene terephthalate nanoplastic pollutants: Characterization and toxicology assessment, *ACS Nano*, 2018, **12**, 7690–7700.

33 S. Lambert and M. Wagner, Characterisation of nanoplastics during the degradation of polystyrene, *Chemosphere*, 2016, **145**, 265–268.

34 S. Lambert and M. Wagner, Formation of microscopic particles during the degradation of different polymers, *Chemosphere*, 2016, **161**, 510–517.

35 L. Eitzen, S. Paul, U. Braun, K. Altmann, M. Jekel and A. Sebastian, The challenge in preparing particle suspensions for aquatic microplastic research, *Environ. Res.*, 2019, **168**, 490–495.

36 M. T. Ekvall, M. Lundqvist, E. Kelpsiene, E. Šileikis, S. B. Gunnarsson and T. Cedervall, Nanoplastics formed during the mechanical breakdown of daily-use polystyrene products, *Nanoscale Adv.*, 2019, **1**, 1055–1061.

37 H. El Hadri, J. Gigault, B. Maxit, B. Grassl and S. Reynaud, Nanoplastic from mechanically degraded primary and secondary microplastics for environmental assessments, *NanoImpact*, 2020, **17**, 100206.

38 N. Liu, M. Tang and J. Ding, The interaction between nanoparticles-protein corona complex and cells and its toxic effect on cells, *Chemosphere*, 2020, **245**, 125624.

39 P. M. Gopinath, V. Saranya, S. Vijayakumar, M. Mythili Meera, S. Ruprekha, R. Kunal, A. Pranay, J. Thomas, A. Mukherjee and N. Chandrasekaran, Assessment on interactive prospectives of nanoplastics with plasma proteins and the toxicological impacts of virgin, coronated and environmentally released-nanoplastics, *Sci. Rep.*, 2019, **9**, 1–15.

40 S. Kihara, S. Ghosh, D. R. McDougall, A. E. Whitten, J. P. Mata, I. Köper and D. J. McGillivray, Structure of soft and hard protein corona around polystyrene nanoplastics—Particle size and protein types, *Biointerphases*, 2020, **15**, 051002.

41 Y. Tan, X. Zhu, D. Wu, E. Song and Y. Song, Compromised Autophagic Effect of Polystyrene Nanoplastics Mediated by Protein Corona Was Recovered after Lysosomal Degradation of Corona, *Environ. Sci. Technol.*, 2020, **54**, 11485–11493.

42 O. O. Fadare, B. Wan, K. Liu, Y. Yang, L. Zhao and L. H. Guo, Eco-Corona vs Protein Corona: Effects of Humic Substances on Corona Formation and Nanoplastic Particle Toxicity in Daphnia magna, *Environ. Sci. Technol.*, 2020, **54**, 8001–8009.

43 Z. Dong, Y. Hou, W. Han, M. Liu, J. Wang and Y. Qiu, Protein corona-mediated transport of nanoplastics in seawater-saturated porous media, *Water Res.*, 2020, **182**, 115978.

44 X. Li, E. He, B. Xia, Y. Liu, P. Zhang, X. Cao, L. Zhao, X. Xu and H. Qiu, Protein corona-induced aggregation of differently sized nanoplastics: impacts of protein type and concentration, *Environ. Sci.: Nano*, 2021, **8**, 1560–1570.

45 K. E. Wheeler, A. J. Chetwynd, K. M. Fahy, B. S. Hong, J. A. Tochihuitl, L. A. Foster and I. Lynch, Environmental dimensions of the protein corona, *Nat. Nanotechnol.*, 2021, **16**, 617–629.

46 M. P. Monopoli, D. Walczyk, A. Campbell, G. Elia, I. Lynch, F. Baldelli Bombelli and K. A. Dawson, Physical-Chemical aspects of protein corona: Relevance to in vitro and in vivo biological impacts of nanoparticles, *J. Am. Chem. Soc.*, 2011, **133**, 2525–2534.

47 S. Tenzer, D. Docter, S. Rosfa, A. Wlodarski, J. Kuharev, A. Rekik, S. K. Knauer, C. Bantz, T. Nawroth, C. Bier, J. Sirirattanapan, W. Mann, L. Treuel, R. Zellner, M. Maskos,

H. Schild and R. H. Stauber, Nanoparticle size is a critical physicochemical determinant of the human blood plasma corona: A comprehensive quantitative proteomic analysis, *ACS Nano*, 2011, **5**, 7155–7167.

48 R. Madathiparambil Visalakshan, L. E. González García, M. R. Benzigar, A. Ghazaryan, J. Simon, A. Mierczynska-Vasilev, T. D. Michl, A. Vinu, V. Mailänder, S. Morsbach, K. Landfester and K. Vasilev, The Influence of Nanoparticle Shape on Protein Corona Formation, *Small*, 2020, **16**(25), 2000285.

49 M. Lundqvist, J. Stigler, G. Elia, I. Lynch, T. Cedervall and K. A. Dawson, Nanoparticle size and surface properties determine the protein corona with possible implications for biological impacts, *Proc. Natl. Acad. Sci. U. S. A.*, 2008, **105**, 14265–14270.

50 L. Anderson and N. G. Anderson, High resolution two-dimensional electrophoresis of human plasma proteins, *Proc. Natl. Acad. Sci. U. S. A.*, 1977, **74**, 5421–5425.

51 I. Grossi, A. Radeghieri, L. Paolini, V. Porrini, A. Pilotto, A. Padovani, A. Marengoni, A. Barbon, A. Bellucci, M. Pizzi, A. Salvi and G. de Petro, MicroRNA-34a-5p expression in the plasma and in its extracellular vesicle fractions in subjects with Parkinson's disease: An exploratory study, *Int. J. Mol. Med.*, 2021, **47**, 533–546.

52 D. Westmeier, R. H. Stauber and D. Docter, The concept of bio-corona in modulating the toxicity of engineered nanomaterials (ENM), *Toxicol. Appl. Pharmacol.*, 2016, **299**, 53–57.

53 I. Horcas, R. Fernández, J. M. Gómez-Rodríguez, J. Colchero, J. Gómez-Herrero and A. M. Baro, WSXM: A software for scanning probe microscopy and a tool for nanotechnology, *Rev. Sci. Instrum.*, 2007, **78**(1), 013705.

54 M. P. Monopoli, A. S. Pitek, I. Lynch and K. A. Dawson, Formation and characterization of the nanoparticle-protein corona, *Methods Mol. Biol.*, 2013, **1025**, 137–155.

55 G. Alvisi, L. Paolini, A. Contarini, C. Zambarda, V. Di Antonio, A. Colosini, N. Mercandelli, M. Timmoneri, G. Palù, L. Caimi, D. Ricotta and A. Radeghieri, Intersectin goes nuclear: Secret life of an endocytic protein, *Biochem. J.*, 2018, **475**, 1455–1472.

56 S. P. Gundupalli, S. Hait and A. Thakur, A review on automated sorting of source-separated municipal solid waste for recycling, *Waste Manage.*, 2017, **60**, 56–74.

57 J. M. Chalmers and N. J. Everall, *Qualitative and Quantitative Analysis of Plastics, Polymers and Rubbers by Vibrational Spectroscopy*, 2007.

58 L. Paolini, S. Federici, G. Consoli, D. Arceri, A. Radeghieri, I. Alessandri and P. Bergese, Fourier-transform Infrared (FT-IR) spectroscopy fingerprints subpopulations of extracellular vesicles of different sizes and cellular origin, *J. Extracell. Vesicles*, 2020, **9**, 1741174.

59 M. Rani, C. Marchesi, S. Federici, G. Rovelli, I. Alessandri, I. Vassalini, S. Ducoli, L. Borgese, A. Zacco, F. Bilo, E. Bontempi and L. E. Depero, Miniaturized Near-Infrared (MicroNIR) Spectrometer in Plastic Waste Sorting, *Materials*, 2019, **12**, 2740.

60 V. Allen, J. H. Kalivas and R. G. Rodriguez, Post-Consumer Plastic Identification Using Raman Spectroscopy, *Appl. Spectrosc.*, 1999, **53**, 672–681.

61 J. Coates, Interpretation of Infrared Spectra, A Practical Approach, in *Encyclopedia of Analytical Chemistry*, John Wiley & Sons, Ltd, Chichester, UK, 2006.

62 V. M. Zolotarev, Comparison of polystyrene IR spectra obtained by the T, R, ATR, and DR methods, *Opt. Spectrosc.*, 2017, **122**, 749–756.

63 C. M. Hoo, N. Starostin, P. West and M. L. Mecartney, A comparison of atomic force microscopy (AFM) and dynamic light scattering (DLS) methods to characterize nanoparticle size distributions, *J. Nanopart. Res.*, 2008, **10**, 89–96.

64 E. Tomaszewska, K. Soliwoda, K. Kadziola, B. Tkacz-Szczesna, G. Celichowski, M. Cichomski, W. Szmaja and J. Grobelny, Detection limits of DLS and UV-Vis spectroscopy in characterization of polydisperse nanoparticles colloids, *J. Nanomater.*, 2013, **2013**, DOI: 10.1155/2013/313081.

65 C. Gardiner, Y. J. Ferreira, R. A. Dragovic, C. W. G. Redman and I. L. Sargent, Extracellular vesicle sizing and enumeration by nanoparticle tracking analysis, *J. Extracell. Vesicles*, 2013, **2**, 19671.

66 C. Montis, A. Zendrini, F. Valle, S. Busatto, L. Paolini, A. Radeghieri, A. Salvatore, D. Berti and P. Bergese, Size distribution of extracellular vesicles by optical correlation techniques, *Colloids Surf., B*, 2017, **158**, 331–338.

67 B. Vestad, A. Llorente, A. Neurauter, S. Phuyal, B. Kierulf, P. Kierulf, T. Skotland, K. Sandvig, K. B. F. Haug and R. Øvstebø, Size and concentration analyses of extracellular vesicles by nanoparticle tracking analysis: a variation study, *J. Extracell. Vesicles*, 2017, **6**, 1344087.

68 H. Cai, E. G. Xu, F. Du, R. Li, J. Liu and H. Shi, Analysis of environmental nanoplastics: Progress and challenges, *Chem. Eng. J.*, 2021, **410**, 128208.

69 A. Ter Halle, L. Jeanneau, M. Martignac, E. Jardé, B. Pedrono, L. Brach and J. Gigault, Nanoplastic in the North Atlantic Subtropical Gyre, *Environ. Sci. Technol.*, 2017, **51**, 13689–13697.

70 M. Davranche, C. Lory, C. Le Juge, F. Blancho, A. Dia, B. Grassl, H. El Hadri, P. Y. Pascal and J. Gigault, Nanoplastics on the coast exposed to the North Atlantic Gyre: Evidence and traceability, *NanoImpact*, 2020, **20**, 100262.

71 A. Wahl, C. Le Juge, M. Davranche, H. El Hadri, B. Grassl, S. Reynaud and J. Gigault, Nanoplastic occurrence in a soil amended with plastic debris, *Chemosphere*, 2021, **262**, 127784.

72 A. Barth, Infrared spectroscopy of proteins, *Biochim. Biophys. Acta, Bioenerg.*, 2007, **1767**, 1073–1101.

73 E. Casals, T. Pfaller, A. Duschl, G. J. Oostingh and V. Puntes, Time evolution of the nanoparticle protein corona, *ACS Nano*, 2010, **4**, 3623–3632.

74 S. Kihara, N. J. Van Der Heijden, C. K. Seal, J. P. Mata, A. E. Whitten, I. Köper and D. J. McGillivray, Soft and Hard Interactions between Polystyrene Nanoplastics and Human Serum Albumin Protein Corona, *Bioconjugate Chem.*, 2019, **30**, 1067–1076.

75 P. M. Kelly, C. Åberg, E. Polo, A. O'Connell, J. Cookman, J. Fallon, Ž. Krpetić and K. A. Dawson, Mapping protein binding sites on the biomolecular corona of nanoparticles, *Nat. Nanotechnol.*, 2015, **10**, 472–479.

76 J. Allan, S. Belz, A. Hoeveler, M. Hugas, H. Okuda, A. Patri, H. Rauscher, P. Silva, W. Slikker, B. Sokull-Kluettgen, W. Tong and E. Anklam, Regulatory landscape of nanotechnology and nanoplastics from a global perspective, *Regul. Toxicol. Pharmacol.*, 2021, **122**, 104885.

77 M. P. Monopoli, C. Åberg, A. Salvati and K. A. Dawson, Biomolecular coronas provide the biological identity of nanosized materials, *Nat. Nanotechnol.*, 2012, **7**, 779–786.

78 A. J. Kokalj, N. B. Hartmann, D. Drobne, A. Potthoff and D. Kühnel, Quality of nanoplastics and microplastics ecotoxicity studies: Refining quality criteria for nanomaterial studies, *J. Hazard. Mater.*, 2021, **415**, 125751.

79 D. Maiolo, P. Bergese, E. Mahon, K. A. Dawson and M. P. Monopoli, Surfactant Titration of Nanoparticle–Protein Corona, *Anal. Chem.*, 2014, **86**, 12055–12063.